Flatness Defect in Thin Strip Cold Rolling and the Friction Impact on it

Rebecca Nakhoul, Pierre Montmitonnet, Sami Abdelkhalek

Proceedings of NAMRI/SME, Vol. 40, 2012

Flatness Defects in Thin Strip Cold Rolling and the Friction Impact on it

Rebecca Nakhoul, Pierre Montmitonnet
CEMEF, UMR CNRS 7635
MINES ParisTech
Sophia-Antipolis, France

Sami Abdelkhalek
IORC Research Centre
ArcelorMittal
Maizières-les-Metz, France

ABSTRACT
Flatness defects are one of the major problems in strip rolling. They are manifested by a wavy shape on the edge, in the centre or in between. Waves are most of the time transverse, but all directions can be observed. These defects come from the heterogeneity of the stress field and the resulting buckling of the compressive areas out of the roll bite. This paper is based on the approach proposed by [1-3] and [4], and programmed previously [5-7] in the FEM software LAM3/TEC3 [8]. In the present paper, the latter is enhanced and applied to the impact of friction and strip tension on flatness of a rolled thin strip. The study shows e.g. that the optimal setting of Work Roll Bending force (WRB) should be changed when friction varies.

KEYWORDS
Rolling, Thin Strips, Finite Element Method, Friction, Flatness Defect.

INTRODUCTION

In thin sheet metal forming processes, buckling may occur and result in major defects. This is especially the case in rolling of thin strips or sheets, e.g. tinplate in the steel industry or foil in the aluminium industry. The quality of the product is affected by waviness of diverse directions and amplitudes, known as flatness defects (Figure 1) [9].

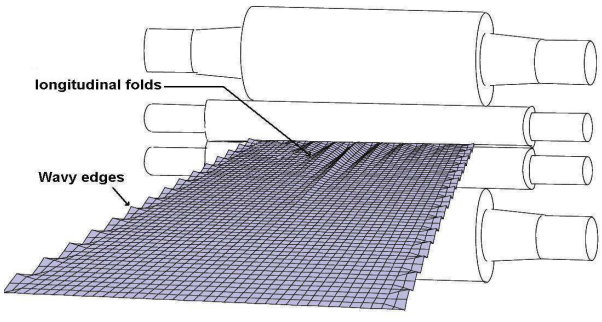

Figure 1. Schematic view of flatness defects during strip rolling.

The origin is the heterogeneous distribution of residual stress: buckling occurs whenever compression exceeds a certain critical value over a significant area. Of course, this out-of-plane displacement can happen only out of the roll bite. Therefore, the measurement of this stress profile by shape-meter rolls (Figure 2) is a central tool in strip shape control. Only the distribution of the longitudinal stress in the transverse direction, $\sigma_{xx}(y)$, can be measured.

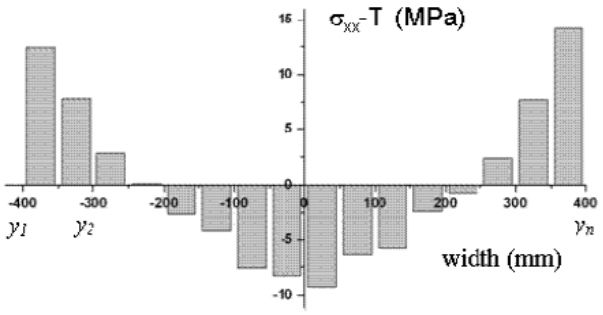

Figure 2. An example of stress profile ("latent flatness") where T is the front tension stress applied on the strip.

On the rolling mill, a high tension stress is applied on the strip ($1/10^{th}$ to $1/4^{th}$ of the yield stress typically). It often prevents the stress profile from transforming into a wavy shape on line, as it brings the stress in the positive range everywhere. In this case, the defect is "latent": it is not eliminated, and may show up as soon as the tension force is cancelled, or upon cutting blanks. It then becomes a "manifested" defect. The term "latent defect" is therefore often used in place of "stress profile", whereas "manifested defect" points to the shape of the sheet.

Inversely, for thinner sheets, part of the defect may show even under tension, with generally very local defects. This paper addresses this situation in priority. A simple approach of buckling has been proposed [1-3] and first implemented in a Finite Difference Method (FDM) context [4], then by two of the present authors [5-7] in a Finite Element Model (FEM) called Lam3/Tec3. It has allowed a fully coupled model to be built. The stress field resulting from rolling is computed, with strip plastic deformation and roll elastic deformation taken into account, and the out-of-bite stress map is examined for buckling in the same model. The stress redistribution due to buckling is a result of this analysis and the effect on the whole system can be studied.

This is different from most of the published, decoupled approaches [10-12] which address the problem in two steps:

- Evaluation, measurement or computation of the (post-bite) residual stress resulting from the plastic deformation of the strip;
- Semi-analytical or shell FEM modelling of the effect of this post-bite stress field for a buckling / post-buckling analysis of the structure.

In the present paper, a summary of the existing model Lam3/Tec3 is presented first. The buckling model is described, and an enhanced algorithm correcting a defect of the method is applied and proven efficient. The coupled model is used to study the effect of friction on the stress profile in a cold rolled thin strip, and to show how flatness actuators (WRB force, strip tension) can be set up for on-line control of (always possible) variations of friction.

THE FEM MODEL LAM3/TEC3

The basis of the present approach is an implicit FEM-based rolling model called Lam3/Tec3, developed in the 90's and early 2000's. It couples strip and roll stack deformation models, as described in [8, 13]. Its general flow chart is given in Figure 3.

For the strip deformation (Lam3), the most salient feature is a *steady state* formulation based on streamline integration to correct the shape for spread, anticipation of deformation at bite entry etc... This can be considered as a variant of Eulerian – Lagrangian formulation. A great care is devoted to the determination of the contact onset and exit, a difficulty in streamline techniques [14], since, due to the space integration, strip surface streamlines may penetrate the roll surface, or on the contrary lose contact artificially.

Another important point is the thermal – mechanical coupling. Due to the high Peclet number (advection dominates conduction heat flow), a Streamline Upwind method is used [15].

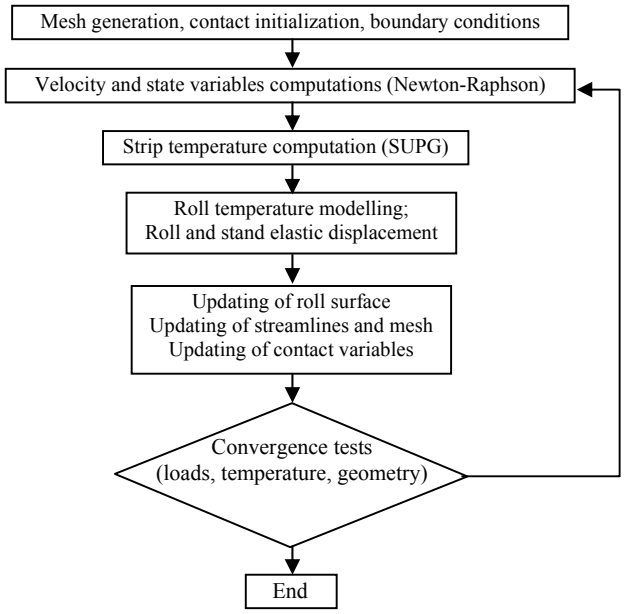

Figure 3. General algorithm of the Lam3/Tec3 FEM strip rolling model.

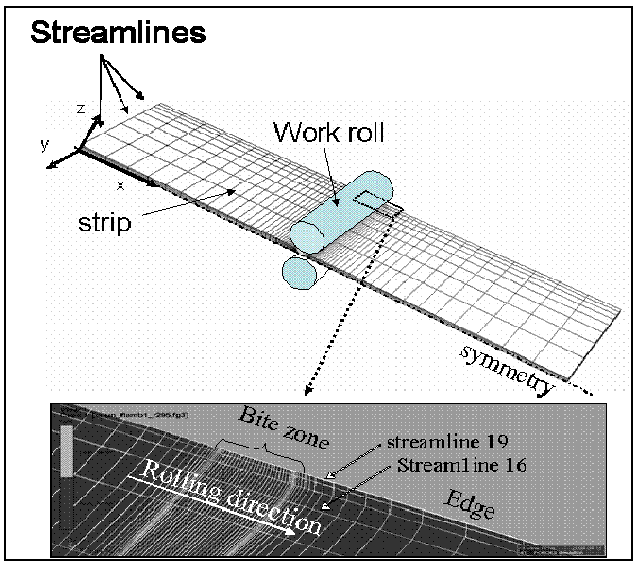

Figure 4. The structured mesh used in Lam3. Note axes x = Rolling Direction [RD], y = Transverse Direction [TD], z = Normal Direction [ND].

As many aspects of the formulation rely on streamlines, a structured mesh has been preferred. It is based on 8-node, tri-linear hexahedra, with reduced integration of the pressure in the Principle of Virtual Power [16]. Figure 4 illustrates the structured mesh, formed by "extrusion in the rolling direction" of a rectangular grid of the upstream plane. Structuring the mesh allows a very efficient local refinement of the mesh, in particular at bite entry and exit.

As residual stresses are essential here, an elastic-viscoplastic constitutive model is used. It is based on Prandtl - Reuss additive decomposition of strain rate. Jaumann objective derivative is used to write the elastic model in rate form, and associated von Mises behaviour is assumed for plasticity. The incremental consistency is based on the standard radial return technique.

In the principle of virtual work, the updated stress is obtained by streamline integration, where the time needed for matter to move from an integration point to the next in the streamline is a substitute for time step [8] – since time does not exist properly speaking in a steady state formulation. As the pseudo-time step is therefore point-dependent due to the adapted mesh, the formulation has been termed "Generalized Heterogeneous Time Stepping" (GHTS).

The roll stack deformation model is another essential feature. Like most of the previous ones [17], the single roll bending and flattening model is based on Timoshenko beam theory, Boussinesq solution for a half-space under general loading, combined after the results in [18]. Based on extensive FEM simulations, corrections have been brought for end effect and the barrel / axle transition. Hertzian contact mechanics is assumed for work roll (WR) / back-up roll (BUR) contact. The Influence Function Method (IFM) is used to discretize the system, with particular refinement near the edge of the strip – WR contact. A global non-linear system is formed with all displacements of all contact lines, with external forces (rolling load, WRB or BURB) in the right-hand side. This non-linear system is solved by Newton-Raphson method. Details can be found in [13].

A SIMPLE BUCKLING MODEL

Principle

Counhaye [4] has proposed a method to deal with sheet buckling in a FDM rolling model, which seems quite similar to the one introduced in a more general context by Roddeman et al. [1]. The same has been implemented in Lam3/Tec3 by Abdelkhalek [5,6].

In [1-3], it is proposed for the membrane theory, and forbids the appearance of a negative stress: every time a negative stress is about to appear, the structure buckles; this means that $\sigma_c = 0$ (σ_c is the critical buckling stress). The following critical conditions are therefore introduced:

$$\begin{aligned} &\vec{n}_1.\sigma.\vec{n}_1 = 0 \\ &\vec{n}_2.\sigma.\vec{n}_2 > 0 \\ &\vec{n}_1.\sigma.\vec{n}_2 = 0 \end{aligned} \qquad (1)$$

where $\vec{n}_1$ and $\vec{n}_2$ are the directions of the principal Cauchy stress tensor in the buckled structure (hence the third equation). This means that when a tension is applied in a direction, the membrane is stiff; if the stress becomes negative, it gets slack and in fact, the corresponding stress is put to 0.

The essence of the model consists in determining an extra deformation which elastically brings the stress in the buckled direction back to 0. It may be interpreted as the shortening of a material line due to buckling of the structure. This is more or less analogous to elastic-plastic decomposition, but is activated only out of the roll bite, i.e. where buckling may manifest.

Practical application

In the context of small incremental deformation, the strain tensor is the sum of two components:

$$\Delta\varepsilon = \Delta\varepsilon^{el} + \Delta\varepsilon^{bu} \qquad (2)$$

where $\Delta\varepsilon^{el}$ is the elastic and $\Delta\varepsilon^{bu}$ is the "buckling strain" increment. Plane stress is assumed (out of bite). If buckling occurs in direction 1 (respectively 2), the following conditions hold:

$$\begin{aligned} &\vec{n}_1.\sigma.\vec{n}_1 = \sigma_c \\ &\vec{n}_2.\sigma.\vec{n}_2 > 0 \\ &\vec{n}_1.\sigma.\vec{n}_2 = 0 \end{aligned} \quad \text{respectively} \quad \begin{aligned} &\vec{n}_1.\sigma.\vec{n}_1 > 0 \\ &\vec{n}_2.\sigma.\vec{n}_2 = \sigma_c \\ &\vec{n}_1.\sigma.\vec{n}_2 = 0 \end{aligned} \qquad (3)$$

The extra deformation representing buckling is computed in the principal axes then transported to the reference frame. Let λ_i, i = I,II be the deformation representing buckling in the principal directions. It is deduced from σ_i, i = I, II as follows:

$$\lambda_i = \frac{\langle \sigma_i - \sigma_c \rangle}{E} \quad i = I, II \qquad (4)$$

Moving back to the reference frame, the buckling strain is added to the global strain increment (u and v are the two in-plane incremental displacements, θ is the angle between principal and reference frames, ν is Poisson's ratio and E is Young's modulus):

$$\Delta\varepsilon_{11} = \frac{\partial u}{\partial x} + \lambda_I \cos^2\theta + \lambda_{II} \sin^2\theta$$
$$\Delta\varepsilon_{22} = \frac{\partial v}{\partial y} + \lambda_{II} \cos^2\theta + \lambda_I \sin^2\theta \quad (5)$$
$$\Delta\varepsilon_{12} = \frac{1}{2}\left(\frac{\partial u}{\partial y} + \frac{\partial v}{\partial x}\right) + \left|\lambda_{II} - \lambda_I\right| \cos\theta \sin\theta$$
$$\Delta\varepsilon_{33} = -\frac{\nu}{1-\nu}(\varepsilon_{11} + \varepsilon_{22})$$

This strain increment replaces the standard one fed into the module solving the constitutive differential equations.

An improved algorithm

The results presented in [5,6] show good agreement with available experimental results, i.e. $\sigma_{xx}(y)$ at the shape-meter roll position, about 1 m after the stand (see Figure 8 below). Yet, it has been noticed that the non-buckling criterion is not respected until ~500 mm after roll bite exit. The numerical result is therefore locally in contradiction with the nature of the model [6]. In the following, a simple 1D analysis of the origin is presented. Let G be a Gauss integration point. The algorithm implemented by Abdelkhalek [5] is such that:

$$\sigma^{(G)} = \sigma^{(G-1)} + \Delta\sigma^{(G)} = \sigma^{(G-1)} + E.\Delta\varepsilon^{el} \quad (6)$$

$\Delta\varepsilon^{el}$ is the elastic strain increment as a material point moves from G-1 to G. From equation (2), $\Delta\varepsilon^{el} = \Delta\varepsilon - \Delta\varepsilon^{bu}$. It was assumed that buckling takes place at the end of the increment:

$$\Delta\varepsilon^{bu} = \frac{\sigma^{(G)} - \sigma_c}{E} \quad (7)$$

Reporting equation (7) into equation (6):

$$\sigma^{(G)} = \frac{\sigma^{(G-1)} + E\Delta\varepsilon + \sigma_c}{2} \neq \sigma_c \quad (8)$$

It shows that this implementation does not lead immediately to the criterion, but decreases the stress gradually – which is indeed observed in the results. A change in the stress integration method along streamlines is proposed to improve this. Considering that $\Delta\varepsilon^{bu}$ occurs during the increment, one may assume:

$$\Delta\varepsilon^{bu} = \frac{\left[\theta\sigma^{(G)} + (1-\theta)\sigma^{(G-1)}\right] - \sigma_c}{E} \quad (9)$$

Recalculating $\sigma^{(G)}$ in the same way shows that if $\theta = 0$:

$$\sigma^{(G)} = E\Delta\varepsilon + \sigma_c \quad (10)$$

In this case, the stress is brought back on the buckling criterion as soon as the strain becomes small. This may not be exactly at exit of the bite, because of a transition zone where the stress reorganizes as the velocity field, heterogeneous at bite exit, evolves to a rigid body movement [7].

Table 1. Simulated rolling operation.

Width of the metal sheet	855 mm
Entry Thickness	0.355 mm
Exit Thickness	0.252 mm
Back and front tension	170 MPa – 100 MPa
Rolling velocity	20.5 m/s
Work roll crown	0.0322% of radius
Sheet crown	4.81% of thickness
Bending force	482 KN
Critical stress σ_c	-10 MPa
Friction Law Coulomb	$\mu = 0.03$
Poisson's ratio	$\nu = 0.3$
Young's modulus	E = 210 GPa

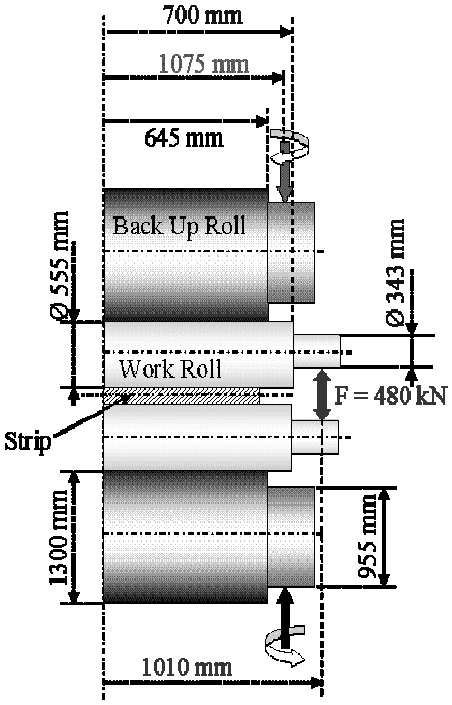

Figure 5. The mill structure (4-Hi) and dimensions.

The algorithm has been modified accordingly. To show the effect of this modification, a rolling operation described in Table 1 and Figure 5 is simulated (the same is used throughout the paper). The critical buckling stress is set to $\sigma_c = -10MPa$.

Results are presented as a comparison between the curves obtained according to equations (6) and (10), focusing on the post-bite area where the inconsistency showed. In Figure 6, only one streamline is shown, but an identical behaviour is found on all streamlines. The new algorithm now practically respects the criterion everywhere. These changes do not affect the global shape of the stress maps, as shown by the stress profile downstream (Figure 7). Figure 8 shows that this stress profile is in good agreement with measurements reported in [4].

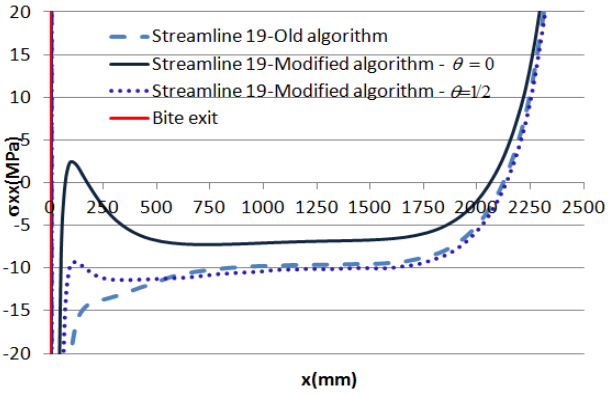

Figure 6. Stress along streamline 19 (edge) after bite exit, before and after the change of integration scheme. Stress scale is zoomed around $\sigma_c = -10MPa$.

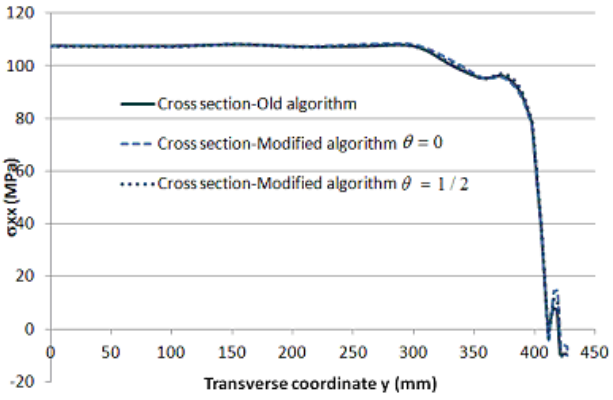

Figure 7. Comparison between the two algorithms on a cross section chosen far from the bite (at shape-meter roll position).

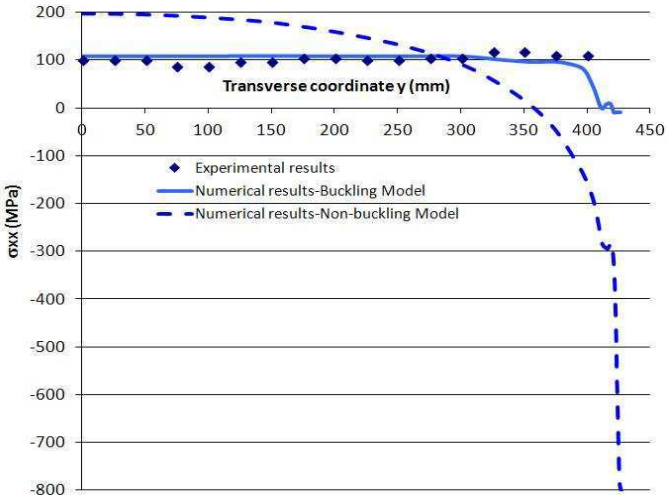

Figure 8. Comparison between the experimental and numerical results (at shape-meter roll position).

APPLICATION: FRICTION AND FLATNESS

As an example of the applicability of this model, the effect of several parameters on the flatness of a thin strip is studied hereafter. The goal is not to provide a complete abacus to run a specific rolling mill, but to highlight interactions between several actuators.

Friction on the one hand, strip tensions on the other hand, have been proved to impact strip profile after cold rolling [19-21]. In [22], the effect of a parabolic variation of friction in the transverse direction has been evaluated. The following study examines the effects of friction, WRB force and strip tension on the shape of the strip. It is shown in particular that for each friction coefficient, there is a best-adapted WRB force in the sense of a minimally heterogeneous stress profile.

Influence of friction on flatness

In this section, a quick study on how friction influences flatness of a thin strip is presented. The rolling operation detailed in Table 1 has been modelled using coefficients of friction between 0.01 and 0.035. Figures 9 and 10 present respectively the strip thickness profile and the stress profile in a cross section about 1 m after roll bite exit.

Figure 9 shows that as friction increases, the thickness of the strip on the edges decreases. Note that a perfect strip gauge control has been assumed, so that the central thickness is maintained at its nominal value. The reason for the growing profile defect is the higher rolling load resulting in more WR bending, hence a thicker centre and a larger edge-drop defect. This occurs in spite of the roll crown, which is normally planned to compensate for bending, but is not adaptable when the roll load varies.

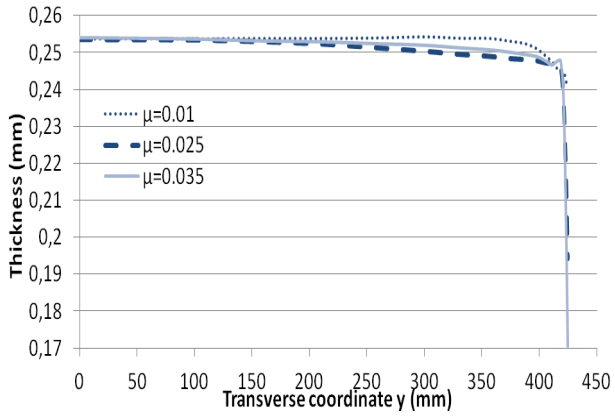

Figure 9. The impact of friction on strip thickness profile.

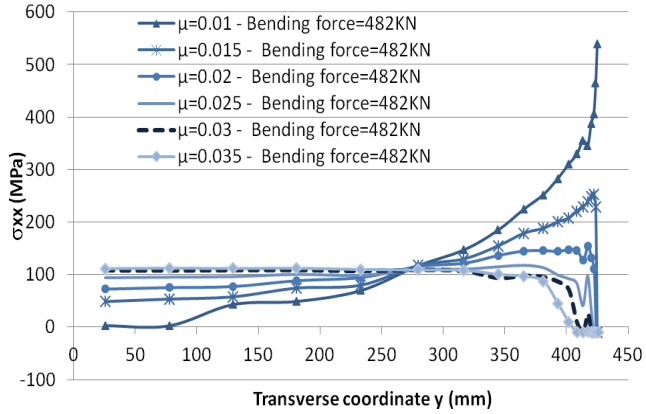

Figure 10. The impact of friction on stress distribution (WRB force = 482 kN).

Proceeding with the stress distribution downstream of the roll bite, Figure 10 shows that changing friction may transform the on-line residual stress distribution in the strip. The profiles must be compared with the average tension 100 MPa: wherever the stress is smaller, there is a suspicion of compression after tension release, therefore of waviness.

For the central value μ = 0.025, the profile is slightly concave in the centre, where σ_{xx} < 100 MPa. The strip might remain flat on the mill, but a wavy centre is not excluded after tension release – wavy edges may also occur simultaneously as the stress there is close to $\sigma_{xx} = 0$.

For the highest friction, μ = 0.035, the tension is slightly above 100 MPa in the centre, rather constant, and drops only in the last 100 mm. The curve is concave except near the edge where waviness of limited dimension might occur. Note that as shown by the roll profiles (Figure 11) and the roll load transverse profile (Figure 12), "roll kiss" has occurred (mutual contact of the two WR on either side of the strip).

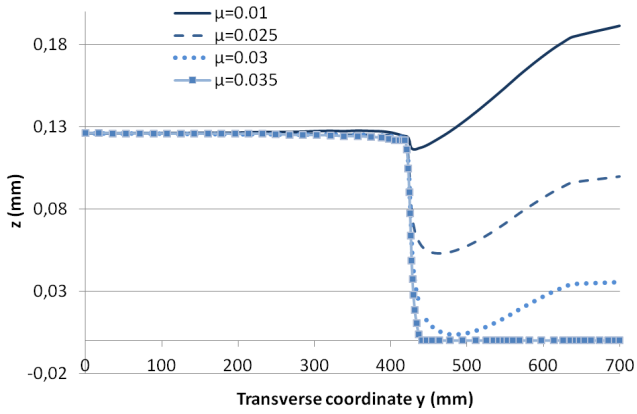

Figure 11. Roll active generator shape z(y), showing flattening and bending.

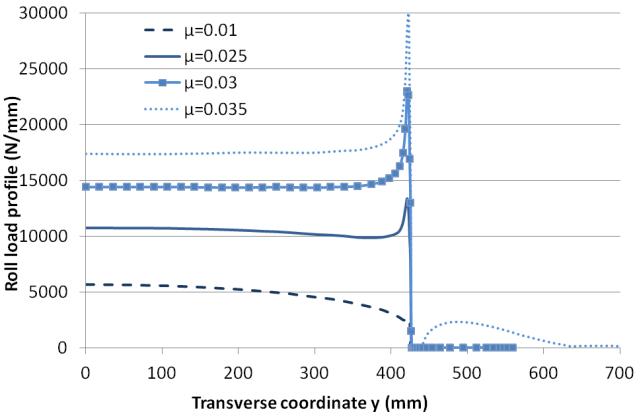

Figure 12. Roll load transverse distribution F(y).

Finally, the lowest friction μ = 0.01 leads to a dramatic change in the stress profile: even under strip tension, the centre is practically slack, whereas the edges are extremely tensile: the WRB force 482 kN, added to the roll crown, is too large for the lower roll load, the gap is thinner in the centre, the elongation of the strip is too large there (this is also where the strip is thickest at entry) and a wavy centre will obviously result. It can be said that the bending force used is poorly adapted to such a low friction.

Best-adapted WR bending force for a given friction level

This analysis shows that friction affects the strip thickness profile, the stress distribution, and will therefore impact the defect type and amplitude. One of the flatness actuators which can be used to improve flatness is the WRB force. Its effect, at constant μ, is pictured in Figure 13. Increasing it to large values clearly exaggerates counter-

bending, with a too large reduction in the centre resulting in a concave profile, leading to a wavy centre.

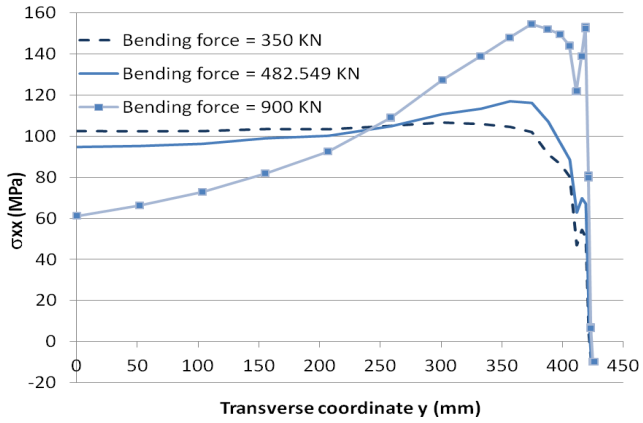

Figure 13. The $\sigma_{xx}(y)$ stress profile for varying bending force and fixed friction coefficient ($\mu = 0.025$).

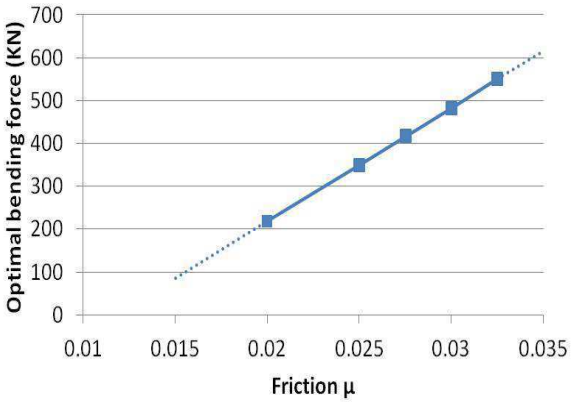

Figure 14. The relationship between friction and optimal bending force.

Thanks to a set of numerical experiments, the relation between friction, bending force and stress profile $\sigma_{xx}(y)$ has been established for the rolling operation investigated. For each value of the friction coefficient, the "optimal bending force" is defined here as the one giving the most flat stress profile (as judged by eye). For instance, from Figure 13, it can be concluded that 350 kN is the optimal bending force for $\mu = 0.025$. Inversely, in Figure 10, F = 482 kN gives a flat profile with $\mu = 0.03$, so that the optimal bending force for $\mu = 0.03$ is 482 kN. The results obtained for the whole range of parameters are given in Figure 14. It shows how the bending force could be preset as a function of friction when the latter varies, e.g. during mill acceleration or deceleration.

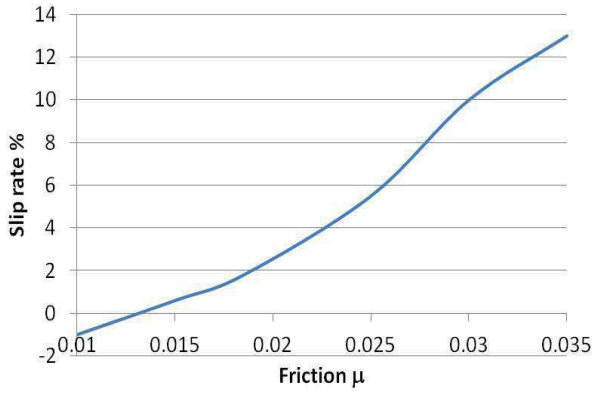

Figure 15. Evolution of the slip rate as friction changes.

The relationship has been established for $\mu = 0.02$ to 0.035. $\mu < 0.02$ is not desirable, due to a risk of skidding shown by the negative forward slip below $\mu = 0.015$ in Figure 15. "High" friction, $\mu > 0.03$, leads to 'Roll Kiss'.

The effect of strip tension on the stress profile

Another possible actuator is the strip tension itself. It is examined in the following if, for a given rolling operation, it can be used to control – and minimize - the stress variations $\sigma_{xx}(y)$. Average tension stresses of 50 and 150 MPa have been tested. Curves of Figures 16 and 17 present respectively the stress profile (average tension T has been subtracted) and the strip thickness profile in a cross section ~1 m after roll bite exit.

Decreasing the tension (50 MPa) does not change the stress profile too much, but increasing it above 100 MPa clearly affects the stress distribution (Figure 16). As tension increases, the stress on the edge is kept at the buckling threshold (-10 MPa), but in relative terms, it is more compressive after tension subtraction. Increasing the tension to 150 MPa increases $\sigma_{xx}(y)$ everywhere, but the profile is almost three times more concave, suggesting a wavy centre upon cancellation of the tension force.

Figure 17 shows that as the tension decreases, the thickness of the strip on the edges decreases (the edge-drop defect is larger). This is because lower tension results in increased roll load, giving more roll flattening, also shown by the large peak at the edge of the roll load profile (Figure 18). The total rolling force increases linearly from 8380 to 9180 and to 10100 kN as tension decreases from 150 to 100 and to 50 MPa.

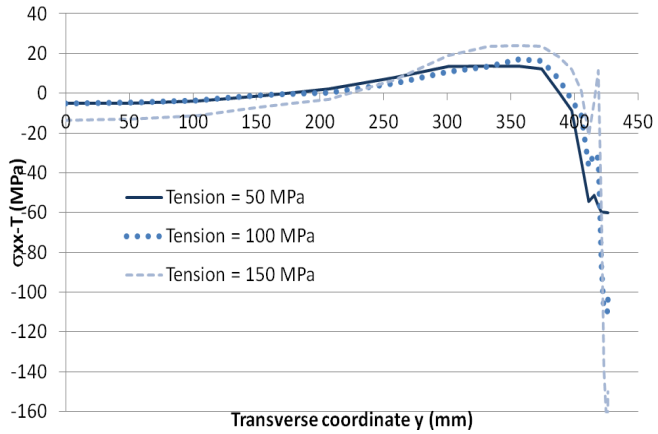

Figure 16. The effect of increasing strip tension on the stress profile (μ = 0.025, WRB force = 482 kN). Strip tension stress T has been subtracted for easier comparison.

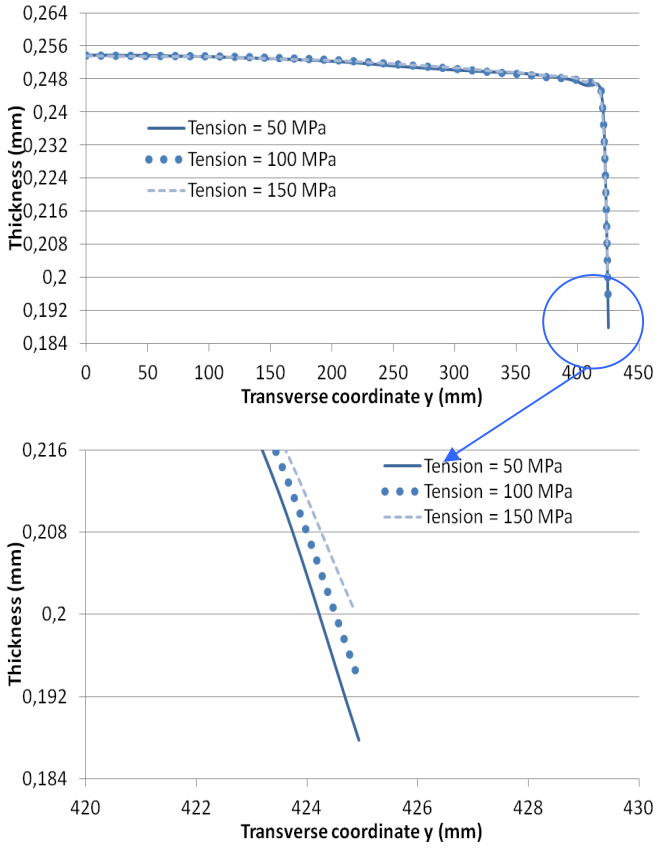

Figure 17. The effect of increasing strip tension on the thickness profile of the strip (μ = 0.025, WRB force = 482 kN).

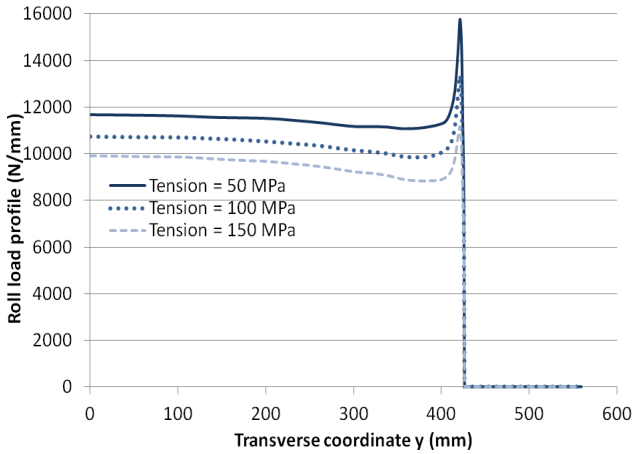

Figure 18. The effect of increasing strip tension on the roll load transverse distribution F(y) (μ = 0.025, WRB force = 482 kN).

CONCLUSION

The problem of flatness defects has been addressed using a completely coupled model combining the FEM for strip elastic-viscoplastic deformation, a powerful semi-analytical model of roll elastic deformation, and a simple model of buckling based on elastic / buckling deformation decomposition. The main result addressing flatness is the computed stress distribution downstream of the roll bite, together with the buckling indicator λ. The stress map is shown consistent with the buckling stress criterion. The stress profile at the position of shape-meter rolls is in good agreement with measurements reported in [4] (see Figure 8). A study of the effect of friction concludes that, in the thin sheet (tinplate) case, friction is an essential parameter for flatness. An adaptive set up of the bending force is shown to be able to compensate for unavoidable friction variations: to each coefficient of friction corresponds a bending force ensuring the best possible flatness. For the time being, the expected optimal flatness is judged only by the homogeneity of the stress profile, but this criterion could be refined in the future.

Front tension has been studied as well. The effect of an increased tension is positive on the roll load and roll deformation, but raises a flatness issue. Probably, this could be again partly compensated by changing simultaneously the WRB force. Playing with two actuators together however raises the question of the local / global character of their effects.

In this study, the effect of $\Delta\varepsilon^{th}$, the thermal dilatation strain, has not been investigated. In a thin strip cold rolling problem, the temperature increase in the roll bite may reach 100 K, and, due to the differential reduction, may not be homogeneous. Cooling may also be heterogeneous, with

edges being cooled faster. This may bring in thermo-elastic stresses, which will be the subject of future investigations.

ACKNOWLEDGEMENT

The authors wish to thank the French National Research Agency (ANR) for its financial support and the partners of the Platform Project for the authorization to publish this work.

REFERENCES

[1] Roddeman DG, Drukker J, Oomens CWJ, Janssen JD (1987) The Wrinkling of Thin Membranes: Part I-Theory. *ASME Trans., J. Appl. Mech.* 54, 884-887.

[2] Roddeman DG, Drukker J, Oomens CWJ, Janssen JD (1987) The Wrinkling of Thin Membranes: Part II-Numerical Analysis. *ASME Trans., J. Appl. Mech.* 54, 888-892.

[3] Roddeman DG (1991) Finite Element Analysis of Wrinkling Membranes. *Comm. Appl. Numer. Meth.* 7, 299-307.

[4] Counhaye C (2000) *Modélisation et contrôle industriel de la géométrie des aciers laminés à froid*. PhD Thesis, Liège University (in French).

[5] Abdelkhalek S (2010) *Un exemple de flambage sous contraintes internes: Étude des défauts de planéité en laminage à froid des tôles minces*. PhD Thesis, MINES ParisTech (in French).

[6] Abdelkhalek S, Montmitonnet P, Legrand N, Buessler P (2011) Coupled approach for flatness predictions in thin strip cold rolling. *Int. J. Mech. Sci.* 53, 651-675.

[7] Abdelkhalek S, Zahrouni H, Montmitonnet P, Legrand N, Potier-Ferry M (2011) Manifested flatness predictions in thin strip cold rolling using a general rolling FEM model. *Steel Res. Int*. Sp. Issue ICTP 2011, 111-116.

[8] Hacquin A, Montmitonnet P, Guilleraut JP (1998) A steady state thermo-elastoviscoplastic finite element model of rolling with coupled thermo-elastic roll deformation. *J. Mat. Proc. Tech.* 60, 109-116.

[9] Roberts WL (1983) *Hot Rolling of steels*. Manufacturing Engineering and Materials Processing Series, Vol. 10. Marcel Dekker, New York.

[10] Bush A, Nicholls R, Tunstall J (2001) Stress levels for elastic buckling of rolled strip and plate. *Ironm. Steelm.* 28, 481-484.

[11] Rammerstorfer FG, Fisher FD, Friedl N (2001) Buckling of free infinite strips under residual stress and global tension. *ASME Trans., J. Appl. Mech.* 68, 399-404.

[12] Fisher FD, Rammerstorfer FG, Friedl N, Wisser W (2000) Buckling phenomena related to rolling and levelling of sheet metal. *Int. J. Mech. Sci.* 42, 1887-1910.

[13] Hacquin A, Montmitonnet P, Guillerault JP (1998) A 3D semi-analytical model of rolling stand deformation with finite element validation. *Eur. J. Mech. A (Solids)* 17, 1, 79-106.

[14] Yamada K, Ogawa S, Ataka M (1992) 3D analysis of flat rolling using rigid-plastic FEM coupled with roll deformation analysis. *Proc. Numiform 92*, Chenot JL, Wood RD & Zienkiewicz OC, eds, Balkema, Rotterdam, 1992.

[15] Pardo E, Weckman DC (1990) A fixed grid FE technique for modelling phase change in steady state conduction – advection problems. *Int. J. Num. Meth. Engg* 29, 969-984.

[16] Gratacos P, Montmitonnet P, Chenot JL (1992) An integration scheme for Prandtl-Reuss elastoplastic constitutive equations. *Int. J. Num. Meth. Eng.* 33 (1992) 943-961.

[17] Shohet KN, Townsend NA (1968) Roll bending methods of crown control in four-high plate mills. *J. Iron Steel Inst.* 1088-1098.

[18] Berger B, Pawelski O, Funke P (1976) Die elastische Verformung der Walzen von Vierwalzengerüsten. *Arch. Eisenhüttenwes.* 47, 6, 351-356 (in German).

[19] Jiang ZY, Tieu AK, Zhang XM, Lu C, Sun WH (2003) Finite element simulation of cold rolling of thin strip. *J. Mat. Proc. Tech.* 140, 542–547.

[20] Jiang ZY, Zhu HT, Wei DB, Tieu AK (2007) Asymmetric Cold Rolling of thin Strip with Roll Edge Kiss. *Proc. ICIEA 2007* (Harbin, PR China, May 23-25, 2007), 2781-2786, published by IEEE.

[21] Wang XC, Yang Q, Du XZ, Jiang ZY (2010) Allowable variation of cold-rolled strip transverse profiles in high tension. *Int. J. Minerals, Metallurgy and Materials* 17, 5, 608-616.

[22] Jiang ZY, Xiong SW, Tieu AK, Wang QJ (2008) Modelling of the effect of friction on cold strip rolling. *J. Mat. Proc. Tech.* 201, 85-90.